Measurement of CP observables in B±→ DK±*andB*±→ Dπ±*withD*→ *K*_S$^0K^{\pm}\pi^{\mp}$ decays

Roel Aaij, Carlos Abellán Beteta, Thomas Ackernley, Bernardo Adeva, Marco Adinolfi, Hossein Afsharnia, Christine Angela Aidala, Salvatore Aiola, Ziad Ajaltouni, Simon Akar, et al.

EUROPEAN ORGANIZATION FOR NUCLEAR RESEARCH (CERN)

CERN-EP-2020-015
LHCb-PAPER-2019-044
June 12, 2020

Measurement of *CP* observables in $B^\pm \to DK^\pm$ and $B^\pm \to D\pi^\pm$ with $D \to K^0_S K^\pm \pi^\mp$ decays

LHCb collaboration[†]

Abstract

Measurements of *CP* observables in $B^\pm \to DK^\pm$ and $B^\pm \to D\pi^\pm$ decays are presented, where D represents a superposition of D^0 and $\overline{D}^0$ states. The D meson is reconstructed in the three-body final states $K^0_S K^\pm \pi^\mp$ and $K^0_S K^\mp \pi^\pm$. The analysis uses samples of B mesons produced in proton-proton collisions, corresponding to an integrated luminosity of 1.0, 2.0, and 6.0 fb^{-1} collected with the LHCb detector at centre-of-mass energies of $\sqrt{s} = 7$, 8, and 13 TeV, respectively. These measurements are the most precise to date, and provide important input for the determination of the CKM angle γ.

Published in J. High Energ. Phys. 2020, 58 (2020)

[†]Authors are listed at the end of this paper.

1 Introduction

In the Standard Model (SM), *CP* violation in the hadronic sector is described by the irreducible complex phase of the Cabibbo–Kobayashi–Maskawa (CKM) quark mixing matrix [1,2]. This matrix is unitary, which leads to the condition $V_{ud}V_{ub}^{*}+V_{cd}V_{cb}^{*}+V_{td}V_{tb}^{*}=0$, where V_{ij} is the CKM matrix element relating quark i to quark j. This condition can be represented by a triangle in the complex plane with internal angles α, β, and γ. The angle γ is defined as $\gamma \equiv \arg\left(-V_{ud}V_{ub}^{*}/V_{cd}V_{cb}^{*}\right)$, which is equal to $\arg\left(-V_{us}V_{ub}^{*}/V_{cs}V_{cb}^{*}\right)$ up to $\mathcal{O}(\lambda^4) \sim 10^{-3}$ in the Wolfenstein parameterisation [3], where λ is the sine of the Cabibbo angle [1]. Improving knowledge of γ can be achieved in a theoretically clean manner by studying the interference of $b \to u$ and $b \to c$ transition amplitudes in tree-level b-hadron decays. Such a measurement provides a benchmark against which other flavour observables that are more susceptible to the influence of physics beyond the SM can be compared [4].

A combination of measurements from LHCb currently yields $\gamma = (74.0\,^{+5.0}_{-5.8})^{\circ}$ [5, 6], which is the most precise determination of γ from a single experiment. The precision is dominated by measurements exploiting the $B^+ \to DK^+$ decay,[1] where D indicates a superposition of D^0 and $\overline{D}^0$ mesons reconstructed in a final state common to both. To continue improving the precision on γ, independent measurements can be performed using all suitable D meson final states. Several different final states have thus far been analysed at LHCb, including a previous measurement of the singly Cabibbo-suppressed $D \to K^0_S K^-\pi^+$ and $D \to K^0_S K^+\pi^-$ modes [7]. These decays are reconstructed in two categories by comparing the charge of the pion produced in the D decay with the charge of the B meson; $B^+ \to [K^0_S K^+\pi^-]_D h^+$ decays are thus labelled "Same Sign" (SS), and $B^+ \to [K^0_S K^-\pi^+]_D h^+$ decays are labelled "Opposite Sign" (OS), where $h \in \{\pi, K\}$. This paper reports an update to Ref. [7], measuring *CP* observables in $B^+ \to DK^+$ and $B^+ \to D\pi^+$ decays using the $D \to K^0_S K^+\pi^-$ and $D \to K^0_S K^-\pi^+$ final states. Data corresponding to $6.0\,\text{fb}^{-1}$ of integrated luminosity collected between 2015 and 2018 (Run 2) of data taking is used. The Run 1 dataset collected during 2011 and 2012 and corresponding to an integrated luminosity of $3.0\,\text{fb}^{-1}$ is also reprocessed, to benefit from an improved selection as well as a reappraisal of the backgrounds.

In order to interpret interference effects involving multi-body D-decays, it is necessary to account for the amplitude structure of the Dalitz plot. Instead of employing an amplitude model to describe the contributing partial waves, the CLEO collaboration have made measurements of the effective amplitude and phase variation using a sample of quantum-correlated D decays collected by the CLEO-c experiment [8]. Due to limited sample size, those measurements were performed averaging over large regions of the Dalitz plot, notably defining one of two regions to contain the $D \to K^*(892)^+K^-$ mode. In the present work, results are reported for both the K^{*+} and non-K^{*+} regions of the Dalitz plot, respecting the boundary defined by CLEO-c. The use of external CLEO-c results, which were performed across the full Dalitz plot and within the K^{*+} region, avoids the need to introduce a systematic uncertainty resulting from an amplitude model description.

The paper is organised as follows: Sec. 2 presents the observables to be measured and their relationships to the physics parameters of interest; Sec. 3 discusses the aspects of the detector, trigger, and simulation that are relevant for the measurement; Secs. 4, 5, and 6

[1]The inclusion of charge-conjugate processes is implied throughout, unless otherwise indicated.

describe the candidate selection, the fit to the invariant mass spectra, and the assignment of systematic uncertainties; the observable results are presented in Sec. 7.

2 Formalism

The SS $B^+ \to [K^0_S K^+\pi^-]_D K^+$ decay can proceed via the D^0 or $\overline{D}^0$ states. As such, the total decay amplitude is given by the sum of two interfering amplitudes,

$$A_{K^0_S K^+\pi^-}(\boldsymbol{x}) = A_{D^0}(\boldsymbol{x}) \quad + \quad r_B e^{i(\delta_B+\gamma)} A_{\overline{D}^0}(\boldsymbol{x}), \tag{1}$$

where $\boldsymbol{x}$ represents the Dalitz plot coordinates $(m^2_{K^0_S K}, m^2_{K^0_S \pi})$, $A_{\{D^0,\overline{D}^0\}}(\boldsymbol{x})$ are the D^0 and $\overline{D}^0$ decay amplitudes at a specific point in the $K^0_S K^+\pi^-$ Dalitz plot [9]. The OS $B^+ \to [K^0_S K^-\pi^+]_D K^+$ decay also proceeds via both D^0 and $\overline{D}^0$, with a total decay amplitude given by

$$A_{K^0_S K^-\pi^+}(\boldsymbol{x}) = A_{\overline{D}^0}(\boldsymbol{x}) \quad + \quad r_B e^{i(\delta_B+\gamma)} A_{D^0}(\boldsymbol{x})\,. \tag{2}$$

The amplitude ratio $r_B = \frac{|A(B^+\to D^0 K^+)|}{|A(B^+\to \overline{D}^0 K^+)|} \sim 0.1$ [5,6], and $\delta_B = \arg\left(\frac{A(B^+\to D^0 K^+)}{A(B^+\to \overline{D}^0 K^+)}\right)$ is the strong-phase difference between the B decay amplitudes. To calculate the decay rate in a finite region of the Dalitz plot, the integral of the interference term over that region must be known. In Ref. [8], measurements of quantum-correlated D decays have been used to determine the amplitude ratio, $r_D = \frac{|A(D^0\to K^0_s K^+\pi^-)|}{|A(\overline{D}^0\to K^0_s K^+\pi^-)|}$, and the integral of the interference term directly in the form of a coherence factor, κ_D, and an average strong phase difference, δ_D [10]. The coherence factor is defined as

$$\kappa_D\, e^{-i\delta_D} = \frac{\int A^*_{K^0_S K^-\pi^+}(\boldsymbol{x})\, A_{K^0_S K^+\pi^-}(\boldsymbol{x})\, d\boldsymbol{x}}{\sqrt{\int |A_{K^0_S K^-\pi^+}(\boldsymbol{x})|^2 d\boldsymbol{x}}\,\sqrt{\int |A_{K^0_S K^+\pi^-}(\boldsymbol{x})|^2 d\boldsymbol{x}}}\,. \tag{3}$$

A similar notation also holds for SS and OS $B^+ \to D\pi^+$ decays with the replacements $r_B \to r^\pi_B$ and $\delta_B \to \delta^\pi_B$, where $r^\pi_B \sim 0.015$.

In each Dalitz region, four decay rates are considered in this analysis [11]:

$$\begin{aligned}
N^{DK^\pm}_{\rm SS} &\propto \quad 1 + r_B^2 r_D^2 + 2 r_B r_D \kappa_D \cos(\delta_B \pm \gamma - \delta_D)\,, \\
N^{DK^\pm}_{\rm OS} &\propto \quad r_B^2 + r_D^2 + 2 r_B r_D \kappa_D \cos(\delta_B \pm \gamma + \delta_D)\,, \\
N^{D\pi^\pm}_{\rm SS} &\propto 1 + (r^\pi_B)^2 r_D^2 + 2 r^\pi_B r_D \kappa_D \cos(\delta^\pi_B \pm \gamma - \delta_D)\,, \\
N^{D\pi^\pm}_{\rm OS} &\propto \quad (r^\pi_B)^2 + r_D^2 + 2 r^\pi_B r_D \kappa_D \cos(\delta^\pi_B \pm \gamma + \delta_D)\,.
\end{aligned} \tag{4}$$

Observables constructed from Eq. 4 have sensitivity to γ that depends upon the value of the coherence factor, with a higher coherence corresponding to greater sensitivity. The CLEO-c results [8] show high coherence within the K^{*+} region, defined as $\pm 100\,\mathrm{MeV}/c^2$ around the K^{*+} mass; $\kappa_D = 0.94 \pm 0.12$ and $\delta_D = (-16.6 \pm 18.4)^\circ$ are reported. With $r_D \approx 0.6$ [8], the maximal CP asymmetry that can be expected is 35% in $B^+ \to DK^+$ decays, but only 2% in $B^+ \to D\pi^+$ decays due to the dissimilarity of r_D and r^π_B. Dedicated measurements in the non-K^{*+} region have not yet been made. Eight yields are measured in this analysis, from which seven ratios are constructed as CP observables; each observable

can be related to γ through the decay rates in Eq. 4. The charge asymmetry is measured in four decay modes,

$$A_m^{Dh} = \frac{N_m^{Dh^-} - N_m^{Dh^+}}{N_m^{Dh^-} + N_m^{Dh^+}},$$

where $m \in \{\text{SS,OS}\}$ and $h \in \{\pi, K\}$. The ratios of $B^+ \to DK^+$ and $B^+ \to D\pi^+$ yields, $R_m^{DK/D\pi}$, are determined, and the ratio of SS to OS $B^+ \to D\pi^+$ yields, $R_{SS/OS}$, is also measured. The measurements are reported for the K^{*+} region of the D Dalitz plot as defined above, and outside it; they are not interpreted in terms of γ in this work, as constraints on the B decay hadronic parameters which come from measurements using other D decay modes are necessary at the current level of statistical precision.

3 Detector and simulation

The LHCb detector [12, 13] is a single-arm forward spectrometer covering the pseudorapidity range $2 < \eta < 5$, designed for the study of particles containing b or c quarks. The detector includes a high-precision tracking system consisting of a silicon-strip vertex detector surrounding the pp interaction region, a silicon-strip detector located upstream of a dipole magnet with a bending power of about 4 Tm, and three stations of silicon-strip detectors and straw drift tubes placed downstream of the magnet. The tracking system provides a measurement of the momentum, p, of charged particles with relative uncertainty that varies from 0.5% at low momentum to 1.0% at 200 GeV/c. The minimum distance of a track to a primary vertex (PV), the impact parameter (IP), is measured with a resolution of $(15 + 29/p_{\rm T})$ μm, where $p_{\rm T}$ is the component of the momentum transverse to the beam, in GeV/c. Different types of charged hadrons are distinguished using information from two ring-imaging Cherenkov (RICH) detectors. Photons, electrons and hadrons are identified by a calorimeter system consisting of scintillating-pad and preshower detectors, an electromagnetic and a hadronic calorimeter. Muons are identified by a system composed of alternating layers of iron and multiwire proportional chambers.

The online event selection is performed by a trigger, which consists of a hardware stage, based on information from the calorimeter and muon systems, followed by a software stage, which applies a full event reconstruction. The events considered in the analysis are triggered at the hardware level when either one of the final-state tracks of the signal decay deposits enough energy in the calorimeter system, or when one of the other particles in the event, not reconstructed as part of the signal candidate, fulfils any trigger requirement. At the software stage, it is required that at least one particle should have high $p_{\rm T}$ and high $\chi^2_{\rm IP}$, where $\chi^2_{\rm IP}$ is defined as the difference in the PV fit χ^2 with and without the inclusion of that particle. A multivariate algorithm [14] is used to identify secondary vertices consistent with being a two-, three-, or four-track b-hadron decay. The PVs are fitted with and without the B candidate tracks, and the PV that gives the smallest $\chi^2_{\rm IP}$ is associated with the B candidate.

Simulated events are used to describe the signal mass shapes and compute efficiencies. In the simulation, pp collisions are generated using Pythia [15] with a specific LHCb configuration [16]. Decays of hadronic particles are described by EvtGen [17], in which final-state radiation is generated using Photos [18]. The interaction of the generated particles with the detector, and its response, are implemented using the Geant4 toolkit [19] as described in Ref. [20].

4 Offline selection

Decays of K^0_S mesons to the $\pi^+\pi^-$ final state are reconstructed in two categories, the first containing K^0_S mesons that decay early enough for the pions to be reconstructed in the vertex detector, and the second containing K^0_S mesons that decay later such that track segments of the pions cannot be formed in the vertex detector. These categories are referred to as *long* and *downstream*, respectively. The candidates in the long category have better mass, momentum, and vertex resolution than those in the downstream category, but the downstream category contains more candidates and thus both are used. Herein, B^+ candidates are denoted long or downstream depending on which category of K^0_S candidate is used.

The D (K^0_S) candidates are required to be within $\pm 25\,\mathrm{MeV}/c^2$ ($\pm 15\,\mathrm{MeV}/c^2$) of the known mass [21], and B^+ meson candidates with invariant masses in the interval 5080–5700 MeV/c^2 are retained. The kaons and pions originating from both the B^+ and D decays are required to have p_T in the range 0.5–10 GeV/c and p in the range 5–100 GeV/c. These requirements ensure that the tracks are within the kinematic coverage of the RICH detectors, which are used to provide particle identification (PID) information.

A boosted decision tree (BDT) classifier [22] implementing the gradient boost algorithm is employed to achieve further combinatorial background suppression. The BDT is trained using simulated $B^+ \to Dh^+$ decays as a proxy for signal and a background sample of candidates in data with invariant masses in the range 5900–7200 MeV/c^2 which are not used in the invariant-mass fit (see Sec. 5). The input to the BDT is a set of features that characterise the signal decay. These features can be divided into two categories: (1) properties of any particle, and (2) properties of composite particles only (the D and B^+ candidates). Specifically:

1. p, p_T, and χ^2_IP;
2. decay time, flight distance between production and decay vertex, decay vertex quality, radial distance between the decay vertex and the PV, and the angle between the particle's momentum vector and the line connecting the production and decay vertices.

In addition, a feature that estimates the imbalance of p_T around the B^+ candidate momentum vector is also used in the BDT. It is defined as

$$I_{p_\mathrm{T}} = \frac{p_\mathrm{T}(B^+) - \Sigma p_\mathrm{T}}{p_\mathrm{T}(B^+) + \Sigma p_\mathrm{T}}\,, \tag{5}$$

where the sum is taken over tracks inconsistent with originating from the PV that lie within a cone around the B^+ candidate, excluding tracks used to make the signal candidate. The cone is defined by a circle with a radius of 1.5 units in the plane of pseudorapidity and azimuthal angle expressed in radians. Including the I_{p_T} feature in the BDT training gives preference to B^+ candidates that are isolated from the rest of the event.

Since no PID information is used in the BDT classifier, the efficiency for $B^+ \to DK^+$ and $B^+ \to D\pi^+$ decays is similar, with insignificant variations arising from small differences in the decay kinematics. The selection requirement applied to the BDT response is optimised by minimising the relative statistical uncertainty on the $R_{SS/OS}$ observable, as measured using the fit described in Sec. 5. PID information from the RICH detectors

is used to improve the purity of the $B^+ \to DK^+$ samples. A strict PID requirement is applied to the companion kaon in $B^+ \to DK^+$ to suppress contamination from $B^+ \to D\pi^+$ decays where the companion pion is misidentified as a kaon. The requirement is around 70% efficient, and genuine $B^+ \to DK^+$ decays failing the requirement are placed into the $B^+ \to D\pi^+$ sample. Less than 0.5% of genuine $B^+ \to D\pi^+$ decays pass the kaon PID requirement, and are placed into the $B^+ \to DK^+$ sample. This results in a $B^+ \to D\pi^+$ background of around 5% relative to the correctly identified $B^+ \to DK^+$ signal. Background from the $B^+ \to [K^0_S\pi^+\pi^-]_D h^+$ decay, which has a branching fraction around ten times larger than the signal, is suppressed by placing PID requirements on both the kaon and pion produced in the D decay.

For long K^0_S candidates, the square of the flight distance significance with respect to the PV is required to be greater than 100 to suppress background from $B^+ \to [K^+\pi^-\pi^+\pi^-]_D h^+$ decays. Background from charmless B decays such as $B^+ \to K^0_s K^- K^+ \pi^+$, which peaks at the same invariant mass as the signal, is suppressed by requiring that the flight distance of the D candidate divided by its uncertainty is greater than 2. Where multiple candidates are found in the same event, one candidate is chosen at random, leading to a reduction in the sample size of approximately 2%.

For several quantities used in the selection and analysis of the data, a kinematic fit [23] is imposed on the full B^+ decay chain. Depending on the quantity being calculated, the D and K^0_S candidates may be constrained to have their known masses [21]. The fit also constrains the B^+ candidate momentum vector to point towards the associated PV, defined as the PV for which the candidate has the smallest $\chi^2_{\rm IP}$. These constraints improve the resolution of the calculated quantities, and thus help enhance the separation between signal and background decays. Furthermore, they improve the mass-squared resolution, which is important for identifying the Dalitz region assignment.

The Dalitz plots for selected candidates in the signal region $\pm 25\,\mathrm{MeV}/c^2$ around the B^+ mass are shown in Fig. 1; within this region, background from decays involving no charm meson constitute less than 5% of the total sample. The Dalitz coordinates are calculated from the kinematic fit with all mass constraints applied. A band corresponding to the intermediate state, $D \to K^*(892)^- K^+$ is visible in each plot.

5 Invariant-mass fit

In order to measure the *CP* observables introduced in Sec. 2, an extended binned maximum-likelihood fit to the invariant-mass distributions of the B meson candidates in the range between $5080\,\mathrm{MeV}/c^2$ and $5700\,\mathrm{MeV}/c^2$ is performed. The fit is performed simultaneously to all decay categories, in order to enable sharing of common parameters. A total of 16 categories are included in the fit: (DK, $D\pi$) $\times$ (SS, OS) $\times$ (long, downstream) $\times$ (B^+, B^-). The fit range is between $5080\,\mathrm{MeV}/c^2$ and $5700\,\mathrm{MeV}/c^2$ in the $B^\pm$ candidate invariant mass. The fit is performed separately for candidates within the K^{*+} region and those outside.

To model the invariant-mass distribution, a total fit probability density function (PDF) is created from several signal and background components. Most of these are modelled using simulated signal and background samples reconstructed as the signal decay and passing all selection requirements. The components are:

1. Signal $B^+ \to DK^+$ and $B^+ \to D\pi^+$ decays, described by the sum of two Crystal Ball

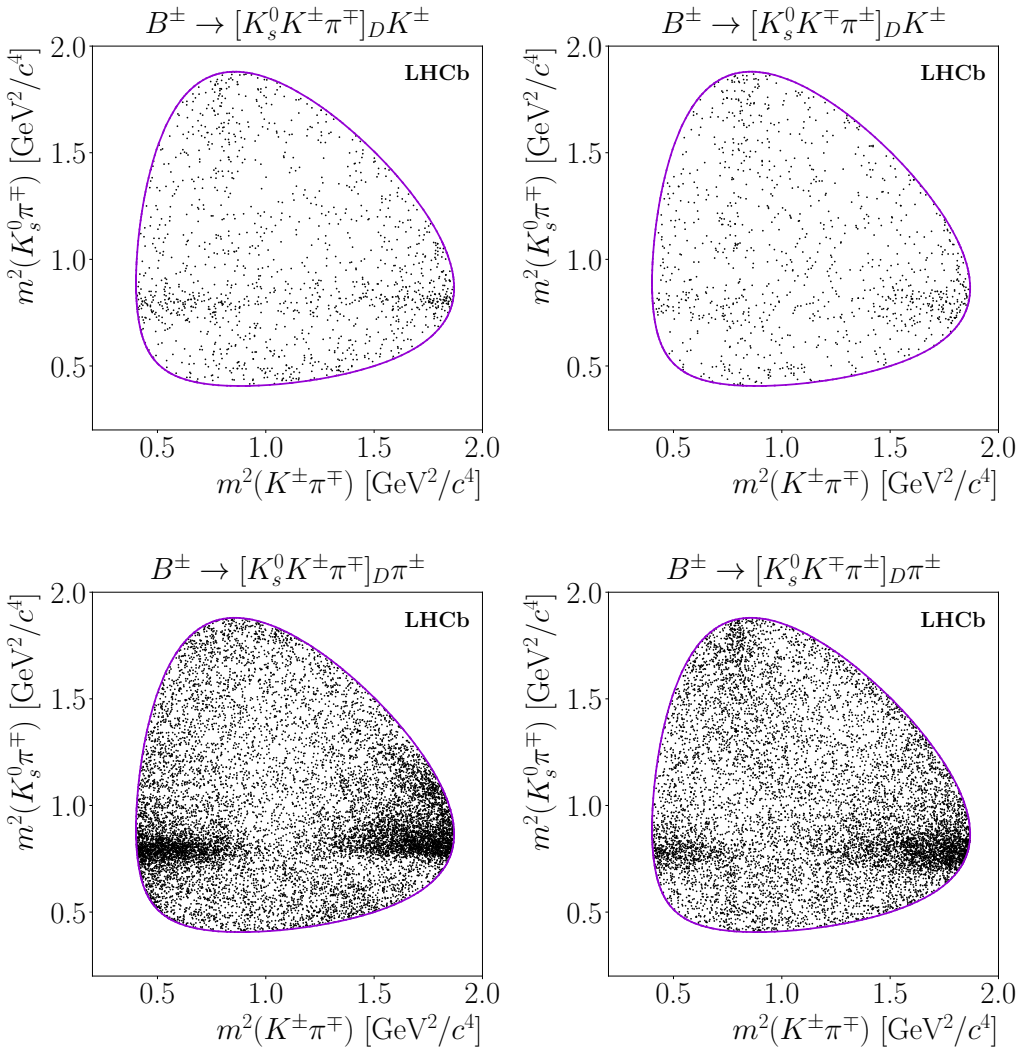

Figure 1: $D \to K^0_S K^+ \pi^-$ Dalitz plots from the SS (left) and OS (right) data samples, for $B^+ \to DK^+$ (top) and $B^+ \to D\pi^+$ (bottom). Both long and downstream K^0_S decays are included. The purple lines indicate the kinematic boundary.

functions [24] with a freely varying common mean and width, and tail parameters fixed from simulation. A single freely varying parameter relates all $B^+ \to DK^+$ widths to their $B^+ \to D\pi^+$ counterparts. SS and OS decays share all shape parameters, but long and downstream decays have separate freely varying widths due to the differences in invariant-mass resolution. All shape parameters are identical for B^+ and B^- decays.

2. Combinatorial background, described by an exponential function with a freely varying exponent in each (SS, OS) $\times$ (long, downstream) category. The combinatorial background yield freely varies in each (DK, $D\pi$) $\times$ (SS, OS) $\times$ (long, downstream) category, but is required to be the same in B^+ and B^-.

3. Partially reconstructed background from the $B^+ \to (D^{*0} \to D\{\pi^0/\gamma\})h^+$, $B^+ \to Dh^+\{\pi^0\}$, and $B^0 \to (D^{*-} \to D\{\pi^-\})h^+$ decays, where the particle in braces is not reconstructed. These components sit at lower invariant-mass values than the

signal, and are described by PDFs constructed from a parabolic function to describe the decay kinematics. This function is convolved with the sum of two Gaussian functions with a common mean in order to describe the detector resolution, as further described in Ref. [25]. All shape parameters are fixed from simulation. All partially reconstructed background yields vary freely, but the $B^0 \to D^{*-}h^+$ component yields are required to be equal in the B^- and B^+ samples; the fast B^0 oscillation renders *CP* violation effects negligible in this time-integrated measurement.

4. Partially reconstructed background from $B_s^0 \to DK^+\{\pi^-\}$ decays, where the pion produced in the B_s^0 decay is not reconstructed, contributes in the $B^+ \to DK^+$ samples. These decays are modelled using a PDF with fixed shape parameters based on the $m(DK)$ distribution observed in Ref. [26]. The yield of this component freely varies in the SS and OS samples, but the yields are required to be equal in the B^- and B^+ samples as the fast B_s^0 oscillation renders *CP* violation effects negligible.

5. Charmless background contributions remain in the $B^+ \to DK^+$ samples after application of the D-meson flight requirement described in Sec. 4. They are estimated using fits to the B^+ candidate invariant-mass distributions in data, where candidates falling in the lower sidebands of the D candidate invariant-mass spectra are considered. The charmless contributions are included as fixed-shape Gaussian functions from simulation, with fixed yields as determined by the sideband fits.

6. Backgrounds from particle misidentification, which arise due to the imperfect efficiency of RICH PID requirements applied to companion hadrons in order to separate $B^+ \to DK^+$ and $B^+ \to D\pi^+$ decays. The efficiencies of the PID requirements are determined using calibration samples of high-purity decays that can be identified without the use of RICH information [27]. Given a PID efficiency $\epsilon^K_{\rm PID} \sim 0.7$ for $B^+ \to DK^+$ decays, a fixed fraction $(1 - \epsilon^K_{\rm PID})$ of the total $B^+ \to DK^+$ signal yield is assigned to a PDF in the corresponding $B^+ \to D\pi^+$ sample. This component is described by a Crystal Ball function with all shape parameters fixed to those found in simulation; due to the companion hadron misidentification, this component falls below the nominal B^+ mass. In the same fashion, a small component is included in the $B^+ \to DK^+$ sample to model misidentified $B^+ \to D\pi^+$ decays, with a yield that freely varies to $\sim 0.4\%$ of the total $B^+ \to D\pi^+$ yield. This component is also described by a Crystal Ball function, with all shape parameters fixed to the values found in simulation.

In order to measure *CP* asymmetries, the detection asymmetries for $K^\pm$ and $\pi^\pm$ mesons must be taken into account. In the fit, a detection asymmetry of $(-0.51 \pm 0.28)\%$ is assigned for each kaon in the final state, primarily due to the fact that the nuclear interaction length of K^- mesons is shorter than that of K^+ mesons. The value used is computed by comparing the charge asymmetries in $D^+ \to K^-\pi^+\pi^+$ and $D^+ \to K^0_{\rm S}\pi^+$ calibration samples, weighted to match the kinematics of the signal kaons [28]. The equivalent asymmetry for pions is smaller, $(-0.06 \pm 0.04)\%$ [29]. All measured *CP* asymmetries are also corrected in the fit for the asymmetry in $B^\pm$ production, which has a value $(+0.14 \pm 0.07)\%$ based on measurements of this quantity made in Refs. [25] and [29].

To measure the $R_{SS}^{DK/D\pi}$ and $R_{OS}^{DK/D\pi}$ observables, the raw signal yields are corrected for small differences in the total efficiency for selecting $B^+ \to DK^+$ and $B^+ \to D\pi^+$

Table 1: Signal yields summed over charge, as measured in each Dalitz region.

	non-K^{*+} region	K^{*+} region
$N_{\rm SS}^{DK^\pm}$	266 ± 27	715 ± 37
$N_{\rm OS}^{DK^\pm}$	336 ± 27	217 ± 22
$N_{\rm SS}^{D\pi^\pm}$	3304 ± 73	8977 ± 106
$N_{\rm OS}^{D\pi^\pm}$	4686 ± 76	3471 ± 66

decays. The efficiency ratio is found to be $\frac{\epsilon(DK)}{\epsilon(D\pi)} = 1.012 \pm 0.016$, which is employed as a fixed correction term in the fit. A similar correction is applied to the $R_{SS/OS}$ observable, to account for differences in selection efficiency for SS and OS decays caused by efficiency variation across the Dalitz plot. The correction is determined using simulated $B^+ \to D\pi^+$ decays and the $D \to K^0_{\rm S}K^+\pi^-$ and $D \to K^0_{\rm S}K^-\pi^+$ amplitudes measured by LHCb in Ref. [30]. The correction is determined in bins across the Dalitz plot, and an average value is calculated to be $\eta = 1.090 \pm 0.008$ (1.007 ± 0.013) within (outside) the K^{*+} region.

Figs. 2–5 show the B meson invariant-mass distributions for all selected candidates, with the results of the fit overlaid; the long and downstream K^0_s categories are shown together. In Tab. 1, the measured signal yields for each D final state are provided for both the K^{*+} and the non-K^{*+} regions. The fit strategy is validated using pseudoexperiments, and is found to be unbiased for all parameters.

6 Systematic uncertainties

All of the *CP* observables measured in this work are constructed as ratios of topologically identical final states. As such, the majority of potential systematic uncertainties cancel with the residual systematic uncertainties detailed here. Small differences in efficiency between $B^+ \to DK^+$ and $B^+ \to D\pi^+$ decays are corrected using simulation as described in Sec. 5, where the uncertainty on the correction arises due to the finite size of the simulated samples. The correction is varied within its uncertainty to determine the systematic uncertainty. The variation in efficiency across the Dalitz plot causes a difference in the total efficiency of SS and OS decays. An appropriate correction is applied to the $R_{SS/OS}$ observable, with an uncertainty arising from the use of a binned procedure to calculate the average correction.

Several fixed shape parameters are used in the fit, including the signal tail parameters and background PDFs. All fixed shape parameters are determined from fits to simulated samples, and are varied to calculate the propagated systematic uncertainty. Charmless backgrounds are modelled as fixed yield components in the invariant-mass fit. The yields are varied within their respective uncertainties to determine the systematic uncertainty. Each charmless component has a fixed *CP* asymmetry of zero in the fit; their asymmetries are independently varied according to a Gaussian of width 0.1 to determine the systematic uncertainty. This width chosen to align with the degree of *CP* asymmetry observed in the charmless background present in measurements of $B^+ \to [h^+h^-]_D h^+$ decays. [25, 31].

All measured *CP* asymmetries are corrected for the $B^\pm$ production asymmetry as well as for the kaon and pion detection asymmetries where relevant. These corrections are applied as fixed terms in the invariant-mass fit, and are varied within their associated

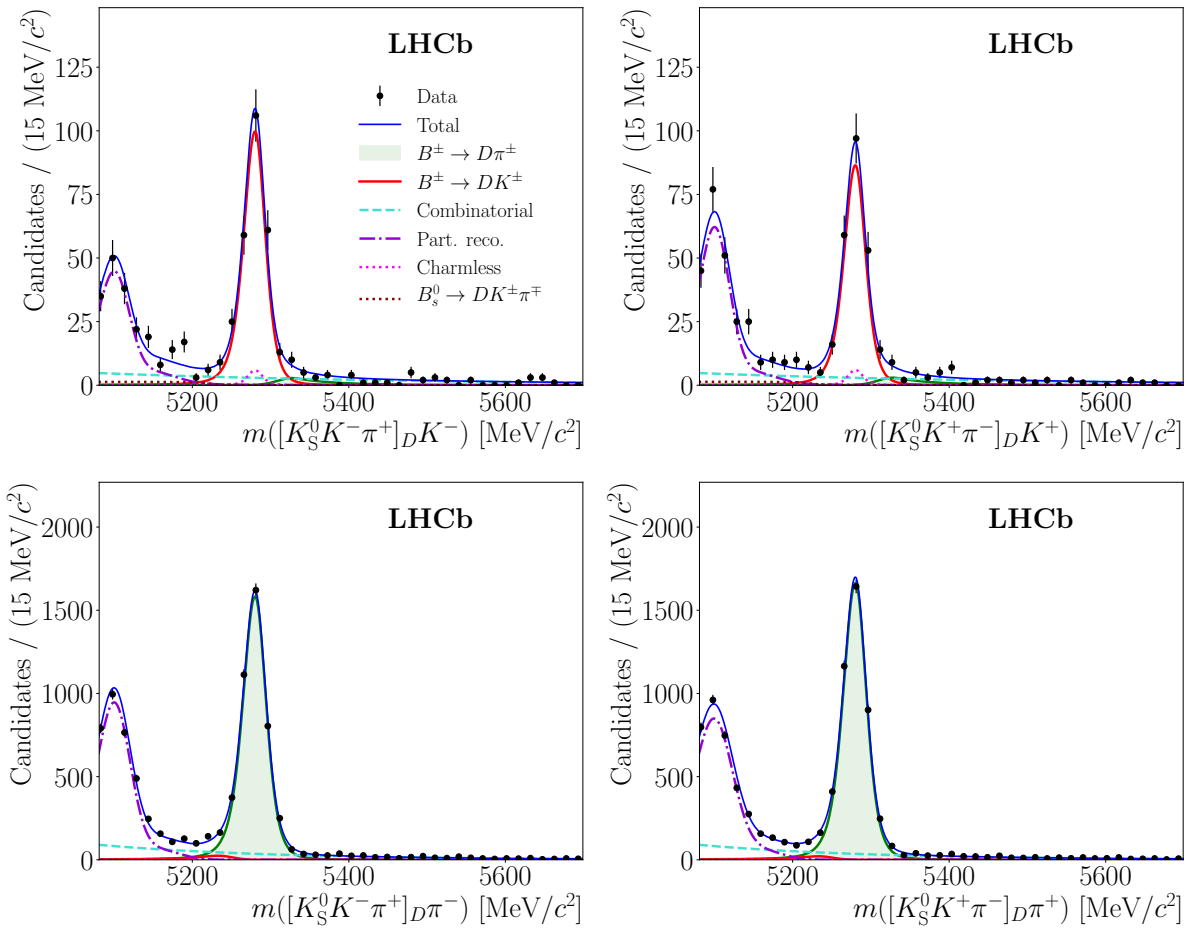

Figure 2: Invariant mass of SS $B^\pm \to [K^0_S K^\pm\pi^\mp]_D h^\pm$ candidates within the K^{*+} region; candidates containing both long and downstream K^0_s mesons are shown.

uncertainties to determine the systematic uncertainty. A fixed PID efficiency is used to determine the fraction of $B^+ \to DK^+$ signal decays that are misidentified as $B^+ \to D\pi^+$. This efficiency is known within 1% relative uncertainty, and is varied within this range to determine the systematic uncertainty.

The systematic uncertainties for each *CP* observable, quoted as a percentage of the statistical uncertainty, are listed in Tabs. 2 and 3. The category *Eff* relates to efficiency corrections, *PDF* to fixed shape parameters, *Cls* to charmless background yields and asymmetries, *Asym* to asymmetry corrections, and *PID* to the PID efficiency. The total systematic uncertainties are given by the sum in quadrature of each contributing systematic.

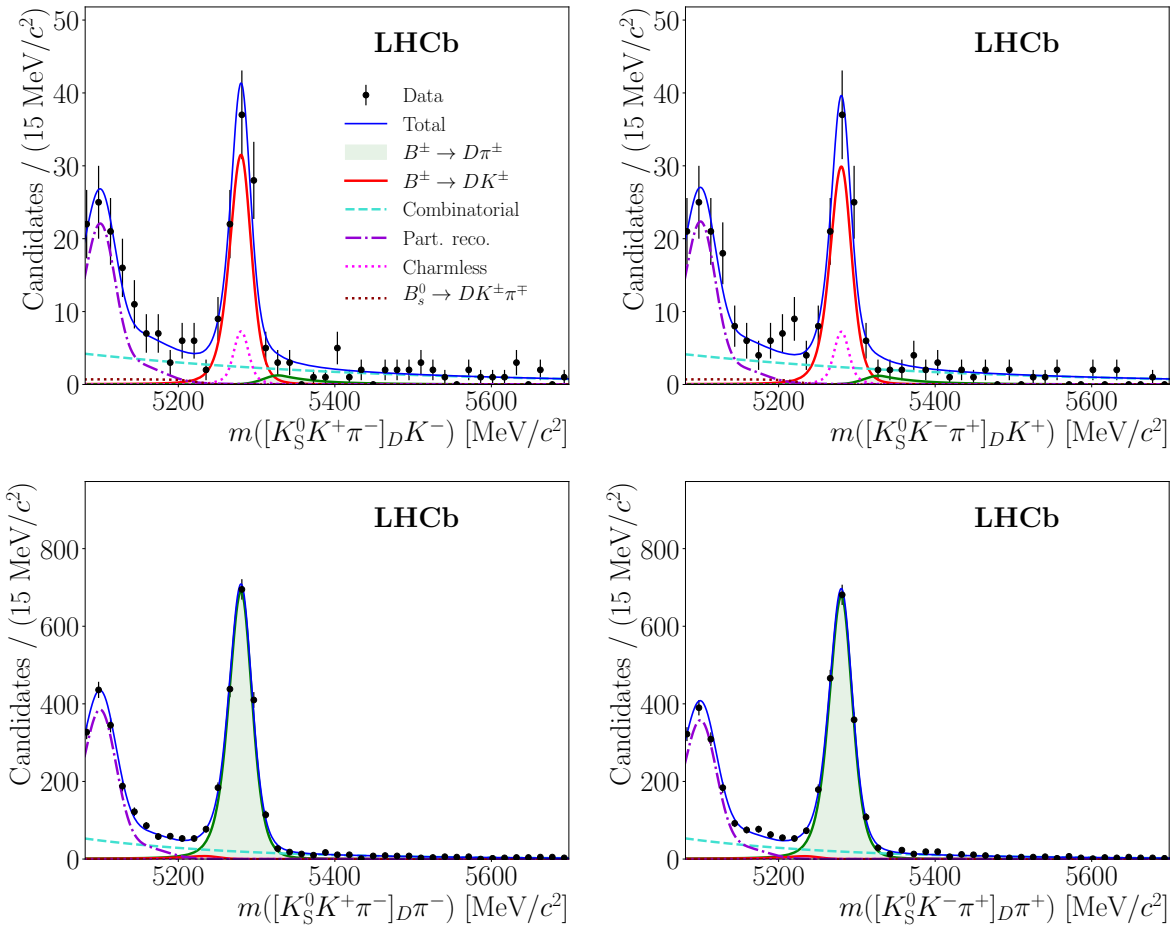

Figure 3: Invariant mass of OS $B^\pm \to [K^0_S K^\mp \pi^\pm]_D h^\pm$ candidates within the K^{*+} region. The fit components are detailed in the legend of Fig. 2.

Table 2: Systematic uncertainties for the K^{*+} region fit. Uncertainties are quoted as a percentage of the statistical uncertainty for a given observable, and the total uncertainty is given by the sum in quadrature of each contribution.

Observable	*Eff*	*PDF*	*Cls*	*Asym*	*PID*	Total
$A_{\rm SS}^{D\pi}$	0.0	0.5	0.4	25.6	0.8	25.6
$A_{\rm OS}^{D\pi}$	0.0	0.4	0.7	16.9	0.9	16.9
$A_{\rm SS}^{DK}$	0.0	1.7	10.1	11.9	6.3	16.9
$A_{\rm OS}^{DK}$	0.0	0.3	16.7	1.3	5.5	17.7
$R_{\rm SS/OS}$	33.6	0.5	0.2	0.1	0.5	33.6
$R_{\rm SS}^{DK/D\pi}$	29.2	3.2	31.3	0.1	8.1	43.7
$R_{\rm OS}^{DK/D\pi}$	15.5	2.7	40.9	0.1	4.9	44.1

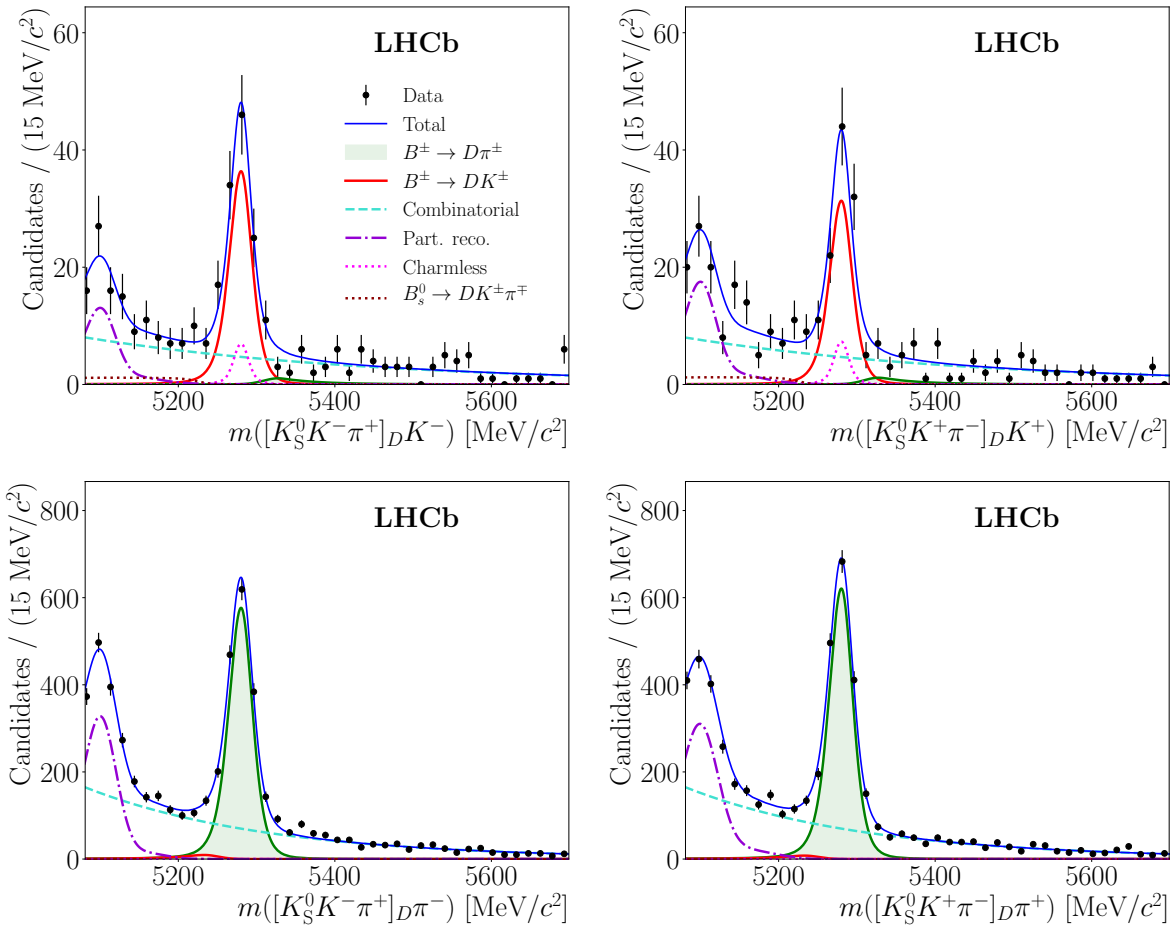

Figure 4: Invariant mass of SS $B^\pm \to [K^0_S K^\pm\pi^\mp]_D h^\pm$ candidates in the non-K^{*+} region. The fit components are detailed in the legend of Fig. 2.

Table 3: Systematic uncertainties for the non-K^{*+} region fit. Uncertainties are quoted as a percentage of the statistical uncertainty for a given observable, and the total uncertainty is given by the sum in quadrature of each contribution.

Observable	*Eff*	*PDF*	*Cls*	*Asym*	*PID*	Total
$A_{\rm SS}^{D\pi}$	0.0	0.4	0.6	14.3	1.0	14.4
$A_{\rm OS}^{D\pi}$	0.0	0.7	0.5	18.4	1.7	18.5
$A_{\rm SS}^{DK}$	0.1	0.5	17.8	7.1	5.8	20.0
$A_{\rm OS}^{DK}$	0.0	1.5	10.9	1.3	9.4	14.5
$R_{\rm SS/OS}$	48.6	0.6	0.5	0.1	0.4	48.6
$R_{\rm SS}^{DK/D\pi}$	14.8	3.0	44.4	0.1	4.4	47.1
$R_{\rm OS}^{DK/D\pi}$	18.6	4.0	32.7	0.1	7.3	38.5

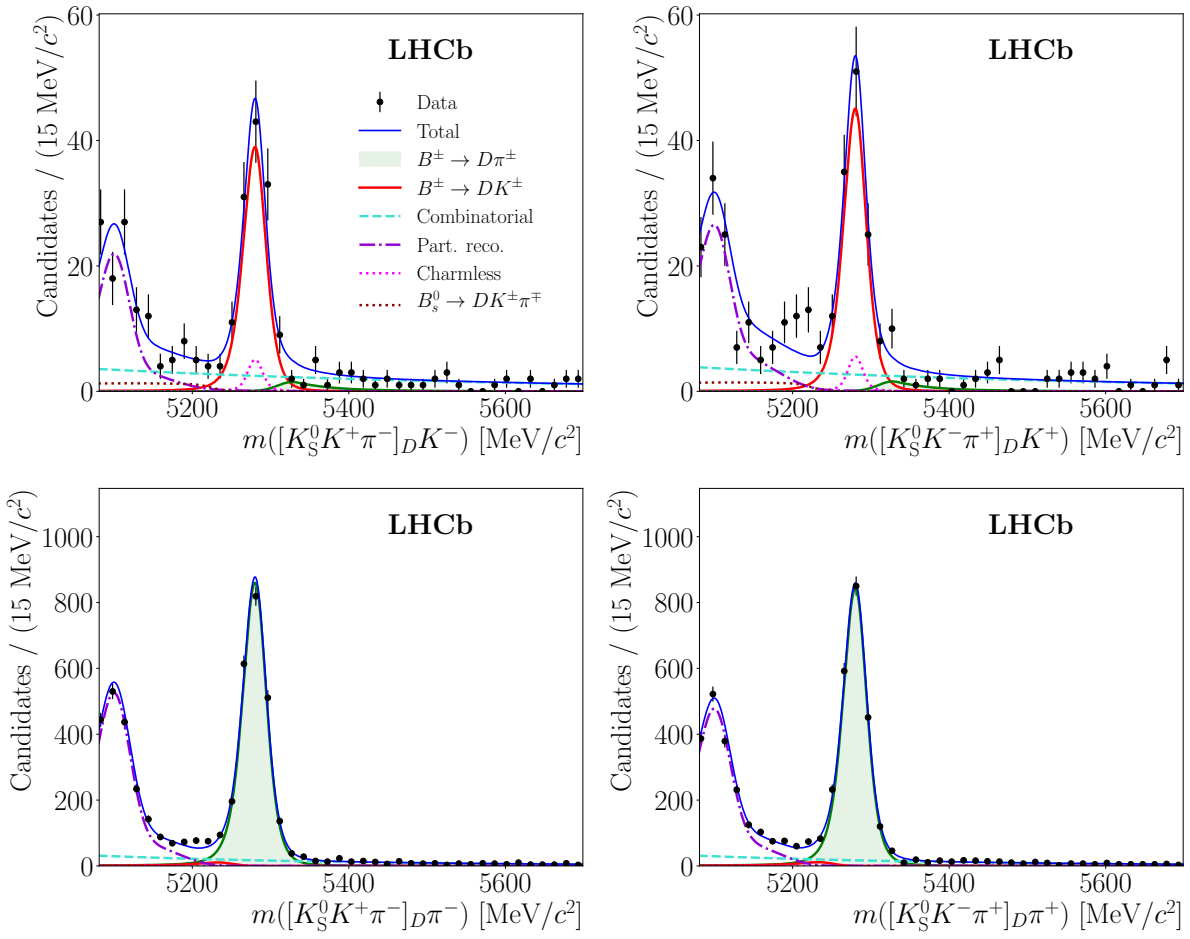

Figure 5: Invariant mass of OS $B^\pm \to [K^0_S K^\mp \pi^\pm]_D h^\pm$ candidates in the non-K^{*+} region. The fit components are detailed in the legend of Fig. 2.

7 Results

The results for the K^{*+} region of the Dalitz plot are

$$\begin{aligned}
A_{\rm SS}^{D\pi} &= -0.020 \pm 0.011 \pm 0.003\,, \\
A_{\rm OS}^{D\pi} &= 0.007 \pm 0.017 \pm 0.003\,, \\
A_{\rm SS}^{DK} &= 0.084 \pm 0.049 \pm 0.008\,, \\
A_{\rm OS}^{DK} &= 0.021 \pm 0.094 \pm 0.017\,, \\
R_{\rm SS/OS} &= 2.585 \pm 0.057 \pm 0.019\,, \\
R_{\rm SS}^{DK/D\pi} &= 0.079 \pm 0.004 \pm 0.002\,, \\
R_{\rm OS}^{DK/D\pi} &= 0.062 \pm 0.006 \pm 0.003\,,
\end{aligned}$$

and the results for the non-K^{*+} region are

$$\begin{aligned}
A_{\rm SS}^{D\pi} &= -0.034 \pm 0.020 \pm 0.003\,, \\
A_{\rm OS}^{D\pi} &= 0.003 \pm 0.015 \pm 0.003\,, \\
A_{\rm SS}^{DK} &= 0.095 \pm 0.089 \pm 0.018\,, \\
A_{\rm OS}^{DK} &= -0.038 \pm 0.075 \pm 0.011\,, \\
R_{\rm SS/OS} &= 0.706 \pm 0.019 \pm 0.009\,, \\
R_{\rm SS}^{DK/D\pi} &= 0.081 \pm 0.008 \pm 0.004\,, \\
R_{\rm OS}^{DK/D\pi} &= 0.073 \pm 0.006 \pm 0.002\,.
\end{aligned}$$

The results are in agreement with Ref. [7], and all statistical uncertainties are reduced in accordance with the increased signal yields. The systematic uncertainties on each asymmetry are reduced considerably due to improved knowledge of the $B^\pm$ production asymmetry and the kaon detection asymmetry. The systematic uncertainties on $R_{SS}^{DK/D\pi}$, $R_{OS}^{DK/D\pi}$, and $R_{SS/OS}$ are also reduced, due to the use of larger simulated samples. All observables are statistically limited with the current data set. The statistical and systematic correlation matrices for the *CP* observables are given in App. A.

A comparison of the K^{*+} region results with the SM expectation is made by calculating the *CP* observables from the current best-fit values of $\gamma = (74.0^{+5.0}_{-5.8})^\circ$, $\delta_B = (131.2^{+5.1}_{-5.9})^\circ$, and $r_B = (9.89^{+0.51}_{-0.50})\%$ for $B^+ \to DK^+$ decays [5]; no comparison is made using the non-K^{*+} results, since the required charm hadronic parameters have not yet been measured. For $B^+ \to D\pi^+$ decays, where no independent information on r_B^π and δ_B^π is available, the uniform PDFs $180^\circ < \delta_B^\pi < 360^\circ$ and $r_B^\pi < 0.02$ are used. The D-decay parameters are taken from the literature: $r_D^2 = 0.655 \pm 0.007$ and $\delta_D = (-16.6 \pm 18.4)^\circ$ [30]; $\kappa = 0.94 \pm 0.12$ [8]. The small corrections due to D mixing are not considered.

For these inputs, the 68% and 95% confidence-level expectation intervals are displayed in Fig. 6, together with the results presented herein. The dominant uncertainty contribution to the expectation intervals comes from the D-decay parameter inputs. The measurements are found to be compatible with the SM expectation, where the χ^2 per degree of freedom is found to be 1.56 taking into account the uncertainties and correlations of both the measurements and the expected values; the corresponding p-value for rejection of the SM hypothesis is 0.14.

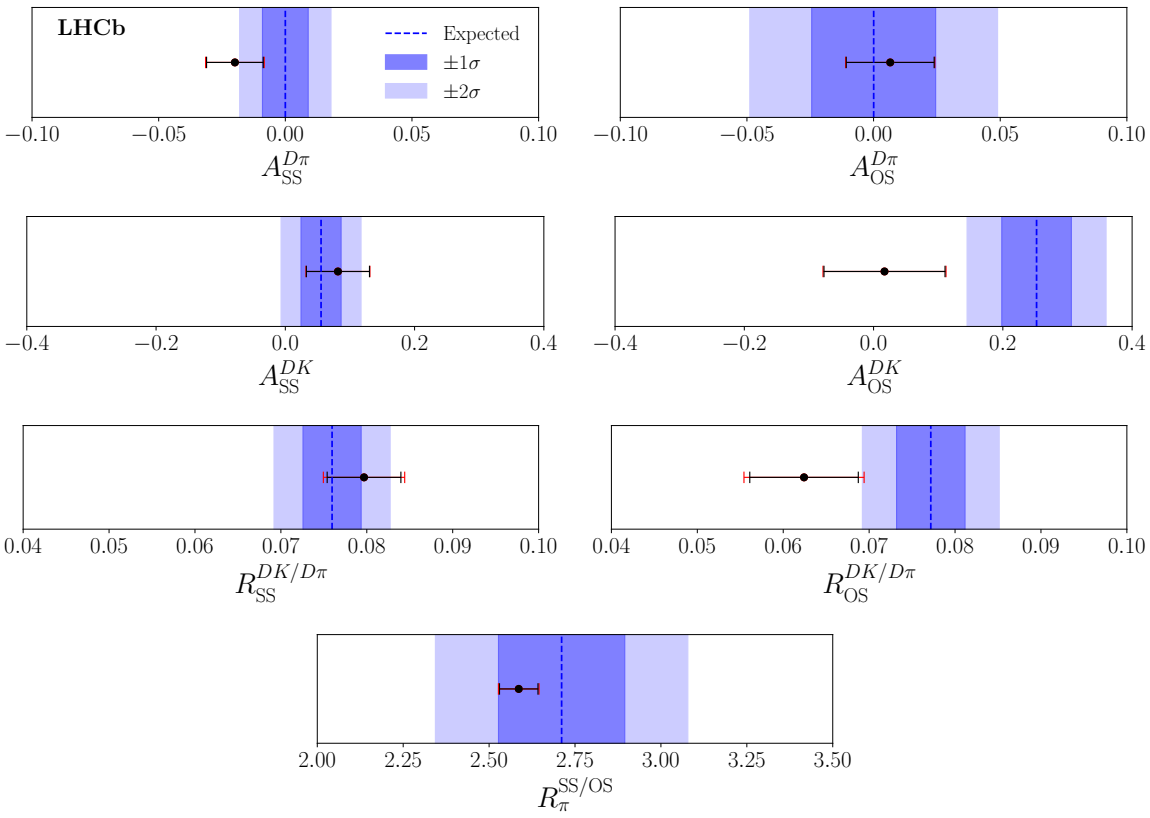

Figure 6: Comparison with SM expectations for results within the K^{*+} region, using current world-average parameter values. The dashed blue line indicates the expected SM value, and the shaded dark (light) blue regions indicate the 68% (95%) confidence-level intervals. The results are shown as black points with black (red) error bars indicating the statistical (total) uncertainty.

8 Conclusion

Measurements of *CP* observables in $B^+ \to DK^+$ and $B^+ \to D\pi^+$ decays with the D meson decaying to $K^0_S K^+\pi^-$ and $K^0_S K^-\pi^+$ are performed using LHCb data collected in Run 1 and Run 2. The results are in agreement with the SM, and supersede those of the previous study [7], benefiting from the increased data sample and improved analysis methods. The measurements presented in this paper improve the precision of several of the *CP* observables used in global fits for γ, which will contribute to improved precision on γ and on the hadronic parameters r_B and δ_B for these decays. Improved measurements of charm hadronic parameters in both the K^{*+} and non-K^{*+} regions would also benefit the interpretation of these results and the constraints on γ that can be obtained from them.

Acknowledgements

We express our gratitude to our colleagues in the CERN accelerator departments for the excellent performance of the LHC. We thank the technical and administrative staff at the LHCb institutes. We acknowledge support from CERN and from the national agencies:

CAPES, CNPq, FAPERJ and FINEP (Brazil); MOST and NSFC (China); CNRS/IN2P3 (France); BMBF, DFG and MPG (Germany); INFN (Italy); NWO (Netherlands); MNiSW and NCN (Poland); MEN/IFA (Romania); MSHE (Russia); MinECo (Spain); SNSF and SER (Switzerland); NASU (Ukraine); STFC (United Kingdom); DOE NP and NSF (USA). We acknowledge the computing resources that are provided by CERN, IN2P3 (France), KIT and DESY (Germany), INFN (Italy), SURF (Netherlands), PIC (Spain), GridPP (United Kingdom), RRCKI and Yandex LLC (Russia), CSCS (Switzerland), IFIN-HH (Romania), CBPF (Brazil), PL-GRID (Poland) and OSC (USA). We are indebted to the communities behind the multiple open-source software packages on which we depend. Individual groups or members have received support from AvH Foundation (Germany); EPLANET, Marie Skłodowska-Curie Actions and ERC (European Union); ANR, Labex P2IO and OCEVU, and Région Auvergne-Rhône-Alpes (France); Key Research Program of Frontier Sciences of CAS, CAS PIFI, and the Thousand Talents Program (China); RFBR, RSF and Yandex LLC (Russia); GVA, XuntaGal and GENCAT (Spain); the Royal Society and the Leverhulme Trust (United Kingdom).

Appendices

A Correlation matrices

Statistical and systematic correlation matrices for the seven *CP* observables are given in Tabs. 4−7, for both the $K^*(892)^\pm$ region and non-$K^*(892)^\pm$ region results.

Table 4: Statistical correlation matrix for the restricted $K^*(892)^\pm$ region fit.

	$A_{\rm SS}^{D\pi}$	$A_{\rm OS}^{D\pi}$	$A_{\rm SS}^{DK}$	$A_{\rm OS}^{DK}$	$R_{\rm SS/OS}$	$R_{\rm SS}^{DK/D\pi}$	$R_{\rm OS}^{DK/D\pi}$
$A_{\rm SS}^{D\pi}$	1	0.00	−0.05	0.00	0.00	−0.01	0.00
$A_{\rm OS}^{D\pi}$	0.00	1	0.00	−0.05	0.00	0.00	0.00
$A_{\rm SS}^{DK}$	−0.05	0.00	1	0.00	0.00	0.00	0.00
$A_{\rm OS}^{DK}$	0.00	−0.05	0.00	1	0.00	0.00	−0.02
$R_{\rm SS/OS}$	0.00	0.00	0.00	0.00	1	−0.11	0.15
$R_{\rm SS}^{DK/D\pi}$	−0.01	0.00	0.00	0.00	−0.11	1	0.06
$R_{\rm OS}^{DK/D\pi}$	0.00	0.00	0.00	−0.02	0.15	0.06	1

Table 5: Systematic correlation matrix for the $K^*(892)^\pm$ region fit.

	$A_{\rm SS}^{D\pi}$	$A_{\rm OS}^{D\pi}$	$A_{\rm SS}^{DK}$	$A_{\rm OS}^{DK}$	$R_{\rm SS/OS}$	$R_{\rm SS}^{DK/D\pi}$	$R_{\rm OS}^{DK/D\pi}$
$A_{\rm SS}^{D\pi}$	1	−0.88	0.74	0.05	0.00	0.00	0.00
$A_{\rm OS}^{D\pi}$	−0.88	1	−0.73	−0.08	0.00	0.00	0.00
$A_{\rm SS}^{DK}$	0.74	−0.73	1	0.63	0.00	−0.17	0.00
$A_{\rm OS}^{DK}$	0.05	−0.08	0.63	1	0.00	0.00	−0.10
$R_{\rm SS/OS}$	0.00	0.00	0.00	0.00	1	0.00	0.00
$R_{\rm SS}^{DK/D\pi}$	0.00	0.00	−0.17	0.00	0.00	1	0.25
$R_{\rm OS}^{DK/D\pi}$	0.00	0.00	0.00	−0.10	0.00	0.25	1

Table 6: Statistical correlation matrix for the non$-K^*(892)^\pm$ region fit.

	$A_{\rm SS}^{D\pi}$	$A_{\rm OS}^{D\pi}$	$A_{\rm SS}^{DK}$	$A_{\rm OS}^{DK}$	$R_{\rm SS/OS}$	$R_{\rm SS}^{DK/D\pi}$	$R_{\rm OS}^{DK/D\pi}$
$A_{\rm SS}^{D\pi}$	1	0.00	−0.03	0.00	0.01	−0.01	0.00
$A_{\rm OS}^{D\pi}$	0.00	1	0.00	−0.05	0.00	0.00	0.00
$A_{\rm SS}^{DK}$	−0.03	0.00	1	0.00	0.00	−0.03	0.00
$A_{\rm OS}^{DK}$	0.00	−0.05	0.00	1	0.00	−0.01	−0.01
$R_{\rm SS/OS}$	0.01	0.00	0.00	0.00	1	−0.16	0.11
$R_{\rm SS}^{DK/D\pi}$	−0.01	0.00	−0.03	−0.01	−0.16	1	0.09
$R_{\rm OS}^{DK/D\pi}$	0.00	0.00	0.00	−0.01	0.11	0.09	1

Table 7: Systematic correlation matrix for the non$-K^*(892)^\pm$ region fit.

	$A_{\rm SS}^{D\pi}$	$A_{\rm OS}^{D\pi}$	$A_{\rm SS}^{DK}$	$A_{\rm OS}^{DK}$	$R_{\rm SS/OS}$	$R_{\rm SS}^{DK/D\pi}$	$R_{\rm OS}^{DK/D\pi}$
$A_{\rm SS}^{D\pi}$	1	−0.84	0.31	0.05	0.00	0.00	0.00
$A_{\rm OS}^{D\pi}$	−0.84	1	−0.35	−0.06	0.00	0.00	0.00
$A_{\rm SS}^{DK}$	0.31	−0.35	1	0.81	0.00	−0.28	0.00
$A_{\rm OS}^{DK}$	0.05	−0.06	0.81	1	0.00	0.00	0.03
$R_{\rm SS/OS}$	0.00	0.00	0.00	0.00	1	0.00	0.00
$R_{\rm SS}^{DK/D\pi}$	0.00	0.00	−0.28	0.00	0.00	1	0.02
$R_{\rm OS}^{DK/D\pi}$	0.00	0.00	0.00	0.03	0.00	0.02	1

References

[1] N. Cabibbo, *Unitary symmetry and leptonic decays*, Phys. Rev. Lett. **10** (1963) 531.

[2] M. Kobayashi and T. Maskawa, *CP-violation in the renormalizable theory of weak interaction*, Prog. Theor. Phys. **49** (1973) 652.

[3] L. Wolfenstein, *Parametrization of the Kobayashi–Maskawa matrix*, Phys. Rev. Lett. **51** (1983) 1945.

[4] D. King, M. Kirk, A. Lenz, and T. Rauh, $|V_{cb}|$ *and* γ *from* B*-mixing*, arXiv:1911.07856.

[5] LHCb collaboration, *Update of the LHCb combination of the CKM angle* γ *using* $B \to DK$ *decays*, LHCb-CONF-2018-002, 2018.

[6] LHCb collaboration, R. Aaij *et al.*, *Measurement of the CKM angle* γ *from a combination of LHCb results*, JHEP **12** (2016) 087, arXiv:1611.03076.

[7] LHCb collaboration, R. Aaij *et al.*, *A study of CP violation in* $B^\pm \to DK^\pm$ *and* $B^\pm \to D\pi^\pm$ *decays with* $D \to K^0_S K^\pm \pi^\mp$ *final states*, Phys. Lett. **B733** (2014) 36, arXiv:1402.2982.

[8] CLEO collaboration, J. Insler *et al.*, *Studies of the decays* $D^0 \to K^0_S K^- \pi^+$ *and* $D^0 \to K^0_S K^+ \pi^-$, Phys. Rev. **D85** (2012) 092016, Erratum ibid. **D94** (2016) 099905, arXiv:1203.3804.

[9] Y. Grossman, Z. Ligeti, and A. Soffer, *Measuring gamma in $B^\pm \to K^\pm (KK^*)_D$ decays*, Phys. Rev. **D67** (2003) 071301, arXiv:hep-ph/0210433.

[10] D. Atwood and A. Soni, *Role of charm factory in extracting CKM phase information via $B \to DK$*, Phys. Rev. **D68** (2003) 033003, arXiv:hep-ph/0304085.

[11] D. Atwood, I. Dunietz, and A. Soni, *Enhanced CP violation with $B \to KD^0(\overline{D}^0)$ modes and extraction of the CKM angle gamma*, Phys. Rev. Lett. **78** (1997) 3257, arXiv:hep-ph/9612433.

[12] LHCb collaboration, A. A. Alves Jr. *et al.*, *The LHCb detector at the LHC*, JINST **3** (2008) S08005.

[13] LHCb collaboration, R. Aaij *et al.*, *LHCb detector performance*, Int. J. Mod. Phys. **A30** (2015) 1530022, arXiv:1412.6352.

[14] V. V. Gligorov and M. Williams, *Efficient, reliable and fast high-level triggering using a bonsai boosted decision tree*, JINST **8** (2013) P02013, arXiv:1210.6861.

[15] T. Sjöstrand, S. Mrenna, and P. Skands, *A brief introduction to PYTHIA 8.1*, Comput. Phys. Commun. **178** (2008) 852, arXiv:0710.3820.

[16] I. Belyaev *et al.*, *Handling of the generation of primary events in Gauss, the LHCb simulation framework*, J. Phys. Conf. Ser. **331** (2011) 032047.

[17] D. J. Lange, *The EvtGen particle decay simulation package*, Nucl. Instrum. Meth. **A462** (2001) 152.

[18] P. Golonka and Z. Was, *PHOTOS Monte Carlo: A precision tool for QED corrections in Z and W decays*, Eur. Phys. J. **C45** (2006) 97, arXiv:hep-ph/0506026.

[19] Geant4 collaboration, J. Allison *et al.*, *Geant4 developments and applications*, IEEE Trans. Nucl. Sci. **53** (2006) 270; Geant4 collaboration, S. Agostinelli *et al.*, *Geant4: A simulation toolkit*, Nucl. Instrum. Meth. **A506** (2003) 250.

[20] M. Clemencic *et al.*, *The LHCb simulation application, Gauss: Design, evolution and experience*, J. Phys. Conf. Ser. **331** (2011) 032023.

[21] Particle Data Group, M. Tanabashi *et al.*, *Review of particle physics*, Phys. Rev. **D98** (2018) 030001.

[22] L. Breiman, J. H. Friedman, R. A. Olshen, and C. J. Stone, *Classification and regression trees*, Wadsworth international group, Belmont, California, USA, 1984.

[23] W. D. Hulsbergen, *Decay chain fitting with a Kalman filter*, Nucl. Instrum. Meth. **A552** (2005) 566, arXiv:physics/0503191.

[24] T. Skwarnicki, *A study of the radiative CASCADE transitions between the Upsilon-Prime and Upsilon resonances*, PhD thesis, Cracow, INP, 1986.

[25] LHCb collaboration, R. Aaij *et al.*, *Measurement of CP observables in $B^\pm \to D^{(*)}K^\pm$ and $B^\pm \to D^{(*)}\pi^\pm$ decays*, Phys. Lett. **B777** (2018) 16, arXiv:1708.06370.

[26] LHCb collaboration, R. Aaij *et al.*, *Dalitz plot analysis of $B^0_s \to \overline{D}^0 K^- \pi^+$ decays*, Phys. Rev. **D90** (2014) 072003, arXiv:1407.7712.

[27] R. Aaij *et al.*, *Selection and processing of calibration samples to measure the particle identification performance of the LHCb experiment in Run 2*, Eur. Phys. J. Tech. Instr. **6** (2018) 1, arXiv:1803.00824.

[28] A. Davis *et al.*, *Measurement of the instrumental asymmetry for $K^-\pi^+$-pairs at LHCb in Run 2*, LHCb-PUB-2018-004, 2018.

[29] LHCb collaboration, R. Aaij *et al.*, *Measurement of the $B^\pm$ production asymmetry and the CP asymmetry in $B^\pm \to J/\psi K^\pm$ decays*, Phys. Rev. **D95** (2017) 052005, arXiv:1701.05501.

[30] LHCb collaboration, R. Aaij *et al.*, *Studies of the resonance structure in $D^0 \to K^0_S K^\pm \pi^\mp$ decays*, Phys. Rev. **D93** (2016) 052018, arXiv:1509.06628.

[31] LHCb collaboration, R. Aaij *et al.*, *Measurement of CP observables in $B^\pm \to DK^\pm$ and $B^\pm \to D\pi^\pm$ with two- and four-body D decays*, Phys. Lett. **B760** (2016) 117, arXiv:1603.08993.

LHCb collaboration

R. Aaij[31], C. Abellán Beteta[49], T. Ackernley[59], B. Adeva[45], M. Adinolfi[53], H. Afsharnia[9], C.A. Aidala[80], S. Aiola[25], Z. Ajaltouni[9], S. Akar[66], P. Albicocco[22], J. Albrecht[14], F. Alessio[47], M. Alexander[58], A. Alfonso Albero[44], G. Alkhazov[37], P. Alvarez Cartelle[60], A.A. Alves Jr[45], S. Amato[2], Y. Amhis[11], L. An[21], L. Anderlini[21], G. Andreassi[48], M. Andreotti[20], F. Archilli[16], A. Artamonov[43], M. Artuso[67], K. Arzymatov[41], E. Aslanides[10], M. Atzeni[49], B. Audurier[11], S. Bachmann[16], J.J. Back[55], S. Baker[60], V. Balagura[11,b], W. Baldini[20,47], A. Baranov[41], R.J. Barlow[61], S. Barsuk[11], W. Barter[60], M. Bartolini[23,47,h], F. Baryshnikov[77], J.M. Basels[13], G. Bassi[28], V. Batozskaya[35], B. Batsukh[67], A. Battig[14], A. Bay[48], M. Becker[14], F. Bedeschi[28], I. Bediaga[1], A. Beiter[67], L.J. Bel[31], V. Belavin[41], S. Belin[26], V. Bellee[48], K. Belous[43], I. Belyaev[38], G. Bencivenni[22], E. Ben-Haim[12], S. Benson[31], S. Beranek[13], A. Berezhnoy[39], R. Bernet[49], D. Berninghoff[16], H.C. Bernstein[67], C. Bertella[47], E. Bertholet[12], A. Bertolin[27], C. Betancourt[49], F. Betti[19,e], M.O. Bettler[54], Ia. Bezshyiko[49], S. Bhasin[53], J. Bhom[33], M.S. Bieker[14], S. Bifani[52], P. Billoir[12], A. Bizzeti[21,u], M. Bjørn[62], M.P. Blago[47], T. Blake[55], F. Blanc[48], S. Blusk[67], D. Bobulska[58], V. Bocci[30], O. Boente Garcia[45], T. Boettcher[63], A. Boldyrev[78], A. Bondar[42,x], N. Bondar[37], S. Borghi[61,47], M. Borisyak[41], M. Borsato[16], J.T. Borsuk[33], T.J.V. Bowcock[59], C. Bozzi[20], M.J. Bradley[60], S. Braun[16], A. Brea Rodriguez[45], M. Brodski[47], J. Brodzicka[33], A. Brossa Gonzalo[55], D. Brundu[26], E. Buchanan[53], A. Büchler-Germann[49], A. Buonaura[49], C. Burr[47], A. Bursche[26], A. Butkevich[40], J.S. Butter[31], J. Buytaert[47], W. Byczynski[47], S. Cadeddu[26], H. Cai[72], R. Calabrese[20,g], L. Calero Diaz[22], S. Cali[22], R. Calladine[52], M. Calvi[24,i], M. Calvo Gomez[44,m], P. Camargo Magalhaes[53], A. Camboni[44,m], P. Campana[22], D.H. Campora Perez[31], A.F. Campoverde Quezada[5], L. Capriotti[19,e], A. Carbone[19,e], G. Carboni[29], R. Cardinale[23,h], A. Cardini[26], I. Carli[6], P. Carniti[24,i], K. Carvalho Akiba[31], A. Casais Vidal[45], G. Casse[59], M. Cattaneo[47], G. Cavallero[47], S. Celani[48], R. Cenci[28,p], J. Cerasoli[10], M.G. Chapman[53], M. Charles[12,47], Ph. Charpentier[47], G. Chatzikonstantinidis[52], M. Chefdeville[8], V. Chekalina[41], C. Chen[3], S. Chen[26], A. Chernov[33], S.-G. Chitic[47], V. Chobanova[45], S. Cholak[48], M. Chrzaszcz[33], A. Chubykin[37], P. Ciambrone[22], M.F. Cicala[55], X. Cid Vidal[45], G. Ciezarek[47], F. Cindolo[19], P.E.L. Clarke[57], M. Clemencic[47], H.V. Cliff[54], J. Closier[47], J.L. Cobbledick[61], V. Coco[47], J.A.B. Coelho[11], J. Cogan[10], E. Cogneras[9], L. Cojocariu[36], P. Collins[47], T. Colombo[47], A. Comerma-Montells[16], A. Contu[26], N. Cooke[52], G. Coombs[58], S. Coquereau[44], G. Corti[47], C.M. Costa Sobral[55], B. Couturier[47], D.C. Craik[63], J. Crkovská[66], A. Crocombe[55], M. Cruz Torres[1,ab], R. Currie[57], C.L. Da Silva[66], E. Dall'Occo[14], J. Dalseno[45,53], C. D'Ambrosio[47], A. Danilina[38], P. d'Argent[47], A. Davis[61], O. De Aguiar Francisco[47], K. De Bruyn[47], S. De Capua[61], M. De Cian[48], J.M. De Miranda[1], L. De Paula[2], M. De Serio[18,d], P. De Simone[22], J.A. de Vries[31], C.T. Dean[66], W. Dean[80], D. Decamp[8], L. Del Buono[12], B. Delaney[54], H.-P. Dembinski[15], A. Dendek[34], V. Denysenko[49], D. Derkach[78], O. Deschamps[9], F. Desse[11], F. Dettori[26,f], B. Dey[7], A. Di Canto[47], P. Di Nezza[22], S. Didenko[77], H. Dijkstra[47], V. Dobishuk[51], F. Dordei[26], M. Dorigo[28,y], A.C. dos Reis[1], L. Douglas[58], A. Dovbnya[50], K. Dreimanis[59], M.W. Dudek[33], L. Dufour[47], G. Dujany[12], P. Durante[47], J.M. Durham[66], D. Dutta[61], M. Dziewiecki[16], A. Dziurda[33], A. Dzyuba[37], S. Easo[56], U. Egede[69], V. Egorychev[38], S. Eidelman[42,x], S. Eisenhardt[57], R. Ekelhof[14], S. Ek-In[48], L. Eklund[58], S. Ely[67], A. Ene[36], E. Epple[66], S. Escher[13], S. Esen[31], T. Evans[47], A. Falabella[19], J. Fan[3], N. Farley[52], S. Farry[59], D. Fazzini[11], P. Fedin[38], M. Féo[47], P. Fernandez Declara[47], A. Fernandez Prieto[45], F. Ferrari[19,e], L. Ferreira Lopes[48], F. Ferreira Rodrigues[2], S. Ferreres Sole[31], M. Ferrillo[49], M. Ferro-Luzzi[47], S. Filippov[40], R.A. Fini[18], M. Fiorini[20,g], M. Firlej[34], K.M. Fischer[62], C. Fitzpatrick[47], T. Fiutowski[34], F. Fleuret[11,b], M. Fontana[47], F. Fontanelli[23,h], R. Forty[47], V. Franco Lima[59], M. Franco Sevilla[65], M. Frank[47], C. Frei[47], D.A. Friday[58], J. Fu[25,q], Q. Fuehring[14], W. Funk[47], E. Gabriel[57], A. Gallas Torreira[45],

D. Galli[19,e], S. Gallorini[27], S. Gambetta[57], Y. Gan[3], M. Gandelman[2], P. Gandini[25], Y. Gao[4], L.M. Garcia Martin[46], J. García Pardiñas[49], B. Garcia Plana[45], F.A. Garcia Rosales[11], L. Garrido[44], D. Gascon[44], C. Gaspar[47], D. Gerick[16], E. Gersabeck[61], M. Gersabeck[61], T. Gershon[55], D. Gerstel[10], Ph. Ghez[8], V. Gibson[54], A. Gioventù[45], O.G. Girard[48], P. Gironella Gironell[44], L. Giubega[36], C. Giugliano[20,g], K. Gizdov[57], V.V. Gligorov[12], C. Göbel[70], E. Golobardes[44,m], D. Golubkov[38], A. Golutvin[60,77], A. Gomes[1,a], P. Gorbounov[38,6], I.V. Gorelov[39], C. Gotti[24,i], E. Govorkova[31], J.P. Grabowski[16], R. Graciani Diaz[44], T. Grammatico[12], L.A. Granado Cardoso[47], E. Graugés[44], E. Graverini[48], G. Graziani[21], A. Grecu[36], R. Greim[31], P. Griffith[20,g], L. Grillo[61], L. Gruber[47], B.R. Gruberg Cazon[62], C. Gu[3], P. A. Günther[16], E. Gushchin[40], A. Guth[13], Yu. Guz[43,47], T. Gys[47], T. Hadavizadeh[62], G. Haefeli[48], C. Haen[47], S.C. Haines[54], P.M. Hamilton[65], Q. Han[7], X. Han[16], T.H. Hancock[62], S. Hansmann-Menzemer[16], N. Harnew[62], T. Harrison[59], R. Hart[31], C. Hasse[14], M. Hatch[47], J. He[5], M. Hecker[60], K. Heijhoff[31], K. Heinicke[14], A.M. Hennequin[47], K. Hennessy[59], L. Henry[46], J. Heuel[13], A. Hicheur[68], D. Hill[62], M. Hilton[61], P.H. Hopchev[48], J. Hu[16], W. Hu[7], W. Huang[5], W. Hulsbergen[31], T. Humair[60], R.J. Hunter[55], M. Hushchyn[78], D. Hutchcroft[59], D. Hynds[31], P. Ibis[14], M. Idzik[34], P. Ilten[52], A. Inglessi[37], K. Ivshin[37], R. Jacobsson[47], S. Jakobsen[47], E. Jans[31], B.K. Jashal[46], A. Jawahery[65], V. Jevtic[14], F. Jiang[3], M. John[62], D. Johnson[47], C.R. Jones[54], B. Jost[47], N. Jurik[62], S. Kandybei[50], M. Karacson[47], J.M. Kariuki[53], N. Kazeev[78], M. Kecke[16], F. Keizer[54,47], M. Kelsey[67], M. Kenzie[55], T. Ketel[32], B. Khanji[47], A. Kharisova[79], K.E. Kim[67], T. Kirn[13], V.S. Kirsebom[48], S. Klaver[22], K. Klimaszewski[35], S. Koliiev[51], A. Kondybayeva[77], A. Konoplyannikov[38], P. Kopciewicz[34], R. Kopecna[16], P. Koppenburg[31], M. Korolev[39], I. Kostiuk[31,51], O. Kot[51], S. Kotriakhova[37], L. Kravchuk[40], R.D. Krawczyk[47], M. Kreps[55], F. Kress[60], S. Kretzschmar[13], P. Krokovny[42,x], W. Krupa[34], W. Krzemien[35], W. Kucewicz[33,l], M. Kucharczyk[33], V. Kudryavtsev[42,x], H.S. Kuindersma[31], G.J. Kunde[66], T. Kvaratskheliya[38], D. Lacarrere[47], G. Lafferty[61], A. Lai[26], D. Lancierini[49], J.J. Lane[61], G. Lanfranchi[22], C. Langenbruch[13], O. Lantwin[49], T. Latham[55], F. Lazzari[28,v], C. Lazzeroni[52], R. Le Gac[10], R. Lefèvre[9], A. Leflat[39], O. Leroy[10], T. Lesiak[33], B. Leverington[16], H. Li[71], L. Li[62], X. Li[66], Y. Li[6], Z. Li[67], X. Liang[67], R. Lindner[47], V. Lisovskyi[14], G. Liu[71], X. Liu[3], D. Loh[55], A. Loi[26], J. Lomba Castro[45], I. Longstaff[58], J.H. Lopes[2], G. Loustau[49], G.H. Lovell[54], Y. Lu[6], D. Lucchesi[27,o], M. Lucio Martinez[31], Y. Luo[3], A. Lupato[27], E. Luppi[20,g], O. Lupton[55], A. Lusiani[28,t], X. Lyu[5], S. Maccolini[19,e], F. Machefert[11], F. Maciuc[36], V. Macko[48], P. Mackowiak[14], S. Maddrell-Mander[53], L.R. Madhan Mohan[53], O. Maev[37,47], A. Maevskiy[78], D. Maisuzenko[37], M.W. Majewski[34], S. Malde[62], B. Malecki[47], A. Malinin[76], T. Maltsev[42,x], H. Malygina[16], G. Manca[26,f], G. Mancinelli[10], R. Manera Escalero[44], D. Manuzzi[19,e], D. Marangotto[25,q], J. Maratas[9,w], J.F. Marchand[8], U. Marconi[19], S. Mariani[21], C. Marin Benito[11], M. Marinangeli[48], P. Marino[48], J. Marks[16], P.J. Marshall[59], G. Martellotti[30], L. Martinazzoli[47], M. Martinelli[24,i], D. Martinez Santos[45], F. Martinez Vidal[46], A. Massafferri[1], M. Materok[13], R. Matev[47], A. Mathad[49], Z. Mathe[47], V. Matiunin[38], C. Matteuzzi[24], K.R. Mattioli[80], A. Mauri[49], E. Maurice[11,b], M. McCann[60], L. Mcconnell[17], A. McNab[61], R. McNulty[17], J.V. Mead[59], B. Meadows[64], C. Meaux[10], G. Meier[14], N. Meinert[74], D. Melnychuk[35], S. Meloni[24,i], M. Merk[31], A. Merli[25], M. Mikhasenko[47], D.A. Milanes[73], E. Millard[55], M.-N. Minard[8], O. Mineev[38], L. Minzoni[20,g], S.E. Mitchell[57], B. Mitreska[61], D.S. Mitzel[47], A. Mödden[14], A. Mogini[12], R.D. Moise[60], T. Mombächer[14], I.A. Monroy[73], S. Monteil[9], M. Morandin[27], G. Morello[22], M.J. Morello[28,t], J. Moron[34], A.B. Morris[10], A.G. Morris[55], R. Mountain[67], H. Mu[3], F. Muheim[57], M. Mukherjee[7], M. Mulder[47], D. Müller[47], K. Müller[49], C.H. Murphy[62], D. Murray[61], P. Muzzetto[26], P. Naik[53], T. Nakada[48], R. Nandakumar[56], T. Nanut[48], I. Nasteva[2], M. Needham[57], N. Neri[25,q], S. Neubert[16], N. Neufeld[47], R. Newcombe[60], T.D. Nguyen[48], C. Nguyen-Mau[48,n], E.M. Niel[11], S. Nieswand[13], N. Nikitin[39], N.S. Nolte[47], C. Nunez[80], A. Oblakowska-Mucha[34], V. Obraztsov[43], S. Ogilvy[58], D.P. O'Hanlon[53], R. Oldeman[26,f], C.J.G. Onderwater[75], J. D. Osborn[80], A. Ossowska[33],

J.M. Otalora Goicochea[2], T. Ovsiannikova[38], P. Owen[49], A. Oyanguren[46], P.R. Pais[48], T. Pajero[28,t], A. Palano[18], M. Palutan[22], G. Panshin[79], A. Papanestis[56], M. Pappagallo[57], L.L. Pappalardo[20,g], C. Pappenheimer[64], W. Parker[65], C. Parkes[61], G. Passaleva[21,47], A. Pastore[18], M. Patel[60], C. Patrignani[19,e], A. Pearce[47], A. Pellegrino[31], M. Pepe Altarelli[47], S. Perazzini[19], D. Pereima[38], P. Perret[9], L. Pescatore[48], K. Petridis[53], A. Petrolini[23,h], A. Petrov[76], S. Petrucci[57], M. Petruzzo[25,q], B. Pietrzyk[8], G. Pietrzyk[48], M. Pili[62], D. Pinci[30], J. Pinzino[47], F. Pisani[19], A. Piucci[16], V. Placinta[36], S. Playfer[57], J. Plews[52], M. Plo Casasus[45], F. Polci[12], M. Poli Lener[22], M. Poliakova[67], A. Poluektov[10], N. Polukhina[77,c], I. Polyakov[67], E. Polycarpo[2], G.J. Pomery[53], S. Ponce[47], A. Popov[43], D. Popov[52], S. Poslavskii[43], K. Prasanth[33], L. Promberger[47], C. Prouve[45], V. Pugatch[51], A. Puig Navarro[49], H. Pullen[62], G. Punzi[28,p], W. Qian[5], J. Qin[5], R. Quagliani[12], B. Quintana[8], N.V. Raab[17], R.I. Rabadan Trejo[10], B. Rachwal[34], J.H. Rademacker[53], M. Rama[28], M. Ramos Pernas[45], M.S. Rangel[2], F. Ratnikov[41,78], G. Raven[32], M. Reboud[8], F. Redi[48], F. Reiss[12], C. Remon Alepuz[46], Z. Ren[3], V. Renaudin[62], S. Ricciardi[56], D.S. Richards[56], S. Richards[53], K. Rinnert[59], P. Robbe[11], A. Robert[12], A.B. Rodrigues[48], E. Rodrigues[64], J.A. Rodriguez Lopez[73], M. Roehrken[47], S. Roiser[47], A. Rollings[62], V. Romanovskiy[43], M. Romero Lamas[45], A. Romero Vidal[45], J.D. Roth[80], M. Rotondo[22], M.S. Rudolph[67], T. Ruf[47], J. Ruiz Vidal[46], A. Ryzhikov[78], J. Ryzka[34], J.J. Saborido Silva[45], N. Sagidova[37], N. Sahoo[55], B. Saitta[26,f], C. Sanchez Gras[31], C. Sanchez Mayordomo[46], R. Santacesaria[30], C. Santamarina Rios[45], M. Santimaria[22], E. Santovetti[29,j], G. Sarpis[61], A. Sarti[30], C. Satriano[30,s], A. Satta[29], M. Saur[5], D. Savrina[38,39], L.G. Scantlebury Smead[62], S. Schael[13], M. Schellenberg[14], M. Schiller[58], H. Schindler[47], M. Schmelling[15], T. Schmelzer[14], B. Schmidt[47], O. Schneider[48], A. Schopper[47], H.F. Schreiner[64], M. Schubiger[31], S. Schulte[48], M.H. Schune[11], R. Schwemmer[47], B. Sciascia[22], A. Sciubba[30,k], S. Sellam[68], A. Semennikov[38], A. Sergi[52,47], N. Serra[49], J. Serrano[10], L. Sestini[27], A. Seuthe[14], P. Seyfert[47], D.M. Shangase[80], M. Shapkin[43], L. Shchutska[48], T. Shears[59], L. Shekhtman[42,x], V. Shevchenko[76,77], E. Shmanin[77], J.D. Shupperd[67], B.G. Siddi[20], R. Silva Coutinho[49], L. Silva de Oliveira[2], G. Simi[27,o], S. Simone[18,d], I. Skiba[20,g], N. Skidmore[16], T. Skwarnicki[67], M.W. Slater[52], J.G. Smeaton[54], A. Smetkina[38], E. Smith[13], I.T. Smith[57], M. Smith[60], A. Snoch[31], M. Soares[19], L. Soares Lavra[9], M.D. Sokoloff[64], F.J.P. Soler[58], B. Souza De Paula[2], B. Spaan[14], E. Spadaro Norella[25,q], P. Spradlin[58], F. Stagni[47], M. Stahl[64], S. Stahl[47], P. Stefko[48], O. Steinkamp[49], S. Stemmle[16], O. Stenyakin[43], M. Stepanova[37], H. Stevens[14], S. Stone[67], S. Stracka[28], M.E. Stramaglia[48], M. Straticiuc[36], S. Strokov[79], J. Sun[26], L. Sun[72], Y. Sun[65], P. Svihra[61], K. Swientek[34], A. Szabelski[35], T. Szumlak[34], M. Szymanski[47], S. Taneja[61], Z. Tang[3], T. Tekampe[14], F. Teubert[47], E. Thomas[47], K.A. Thomson[59], M.J. Tilley[60], V. Tisserand[9], S. T'Jampens[8], M. Tobin[6], S. Tolk[47], L. Tomassetti[20,g], D. Tonelli[28], D. Torres Machado[1], D.Y. Tou[12], E. Tournefier[8], M. Traill[58], M.T. Tran[48], E. Trifonova[77], C. Trippl[48], A. Trisovic[54], A. Tsaregorodtsev[10], G. Tuci[28,47,p], A. Tully[48], N. Tuning[31], A. Ukleja[35], A. Usachov[31], A. Ustyuzhanin[41,78], U. Uwer[16], A. Vagner[79], V. Vagnoni[19], A. Valassi[47], G. Valenti[19], M. van Beuzekom[31], H. Van Hecke[66], E. van Herwijnen[47], C.B. Van Hulse[17], M. van Veghel[75], R. Vazquez Gomez[44,22], P. Vazquez Regueiro[45], C. Vázquez Sierra[31], S. Vecchi[20], J.J. Velthuis[53], M. Veltri[21,r], A. Venkateswaran[67], M. Vernet[9], M. Veronesi[31], M. Vesterinen[55], J.V. Viana Barbosa[47], D. Vieira[64], M. Vieites Diaz[48], H. Viemann[74], X. Vilasis-Cardona[44,m], A. Vitkovskiy[31], A. Vollhardt[49], D. Vom Bruch[12], A. Vorobyev[37], V. Vorobyev[42,x], N. Voropaev[37], R. Waldi[74], J. Walsh[28], J. Wang[3], J. Wang[72], J. Wang[6], M. Wang[3], Y. Wang[7], Z. Wang[49], D.R. Ward[54], H.M. Wark[59], N.K. Watson[52], D. Websdale[60], A. Weiden[49], C. Weisser[63], B.D.C. Westhenry[53], D.J. White[61], M. Whitehead[13], D. Wiedner[14], G. Wilkinson[62], M. Wilkinson[67], I. Williams[54], M. Williams[63], M.R.J. Williams[61], T. Williams[52], F.F. Wilson[56], W. Wislicki[35], M. Witek[33], L. Witola[16], G. Wormser[11], S.A. Wotton[54], H. Wu[67], K. Wyllie[47], Z. Xiang[5], D. Xiao[7], Y. Xie[7], H. Xing[71], A. Xu[4], L. Xu[3],

M. Xu[7], Q. Xu[5], Z. Xu[4], Z. Yang[3], Z. Yang[65], Y. Yao[67], L.E. Yeomans[59], H. Yin[7], J. Yu[7,aa], X. Yuan[67], O. Yushchenko[43], K.A. Zarebski[52], M. Zavertyaev[15,c], M. Zdybal[33], M. Zeng[3], D. Zhang[7], L. Zhang[3], S. Zhang[4], W.C. Zhang[3,z], Y. Zhang[47], A. Zhelezov[16], Y. Zheng[5], X. Zhou[5], Y. Zhou[5], X. Zhu[3], V. Zhukov[13,39], J.B. Zonneveld[57], S. Zucchelli[19,e].

[1] *Centro Brasileiro de Pesquisas Físicas (CBPF), Rio de Janeiro, Brazil*
[2] *Universidade Federal do Rio de Janeiro (UFRJ), Rio de Janeiro, Brazil*
[3] *Center for High Energy Physics, Tsinghua University, Beijing, China*
[4] *School of Physics State Key Laboratory of Nuclear Physics and Technology, Peking University, Beijing, China*
[5] *University of Chinese Academy of Sciences, Beijing, China*
[6] *Institute Of High Energy Physics (IHEP), Beijing, China*
[7] *Institute of Particle Physics, Central China Normal University, Wuhan, Hubei, China*
[8] *Univ. Grenoble Alpes, Univ. Savoie Mont Blanc, CNRS, IN2P3-LAPP, Annecy, France*
[9] *Université Clermont Auvergne, CNRS/IN2P3, LPC, Clermont-Ferrand, France*
[10] *Aix Marseille Univ, CNRS/IN2P3, CPPM, Marseille, France*
[11] *Université Paris-Saclay, CNRS/IN2P3, IJCLab, Orsay, France*
[12] *LPNHE, Sorbonne Université, Paris Diderot Sorbonne Paris Cité, CNRS/IN2P3, Paris, France*
[13] *I. Physikalisches Institut, RWTH Aachen University, Aachen, Germany*
[14] *Fakultät Physik, Technische Universität Dortmund, Dortmund, Germany*
[15] *Max-Planck-Institut für Kernphysik (MPIK), Heidelberg, Germany*
[16] *Physikalisches Institut, Ruprecht-Karls-Universität Heidelberg, Heidelberg, Germany*
[17] *School of Physics, University College Dublin, Dublin, Ireland*
[18] *INFN Sezione di Bari, Bari, Italy*
[19] *INFN Sezione di Bologna, Bologna, Italy*
[20] *INFN Sezione di Ferrara, Ferrara, Italy*
[21] *INFN Sezione di Firenze, Firenze, Italy*
[22] *INFN Laboratori Nazionali di Frascati, Frascati, Italy*
[23] *INFN Sezione di Genova, Genova, Italy*
[24] *INFN Sezione di Milano-Bicocca, Milano, Italy*
[25] *INFN Sezione di Milano, Milano, Italy*
[26] *INFN Sezione di Cagliari, Monserrato, Italy*
[27] *INFN Sezione di Padova, Padova, Italy*
[28] *INFN Sezione di Pisa, Pisa, Italy*
[29] *INFN Sezione di Roma Tor Vergata, Roma, Italy*
[30] *INFN Sezione di Roma La Sapienza, Roma, Italy*
[31] *Nikhef National Institute for Subatomic Physics, Amsterdam, Netherlands*
[32] *Nikhef National Institute for Subatomic Physics and VU University Amsterdam, Amsterdam, Netherlands*
[33] *Henryk Niewodniczanski Institute of Nuclear Physics Polish Academy of Sciences, Kraków, Poland*
[34] *AGH - University of Science and Technology, Faculty of Physics and Applied Computer Science, Kraków, Poland*
[35] *National Center for Nuclear Research (NCBJ), Warsaw, Poland*
[36] *Horia Hulubei National Institute of Physics and Nuclear Engineering, Bucharest-Magurele, Romania*
[37] *Petersburg Nuclear Physics Institute NRC Kurchatov Institute (PNPI NRC KI), Gatchina, Russia*
[38] *Institute of Theoretical and Experimental Physics NRC Kurchatov Institute (ITEP NRC KI), Moscow, Russia, Moscow, Russia*
[39] *Institute of Nuclear Physics, Moscow State University (SINP MSU), Moscow, Russia*
[40] *Institute for Nuclear Research of the Russian Academy of Sciences (INR RAS), Moscow, Russia*
[41] *Yandex School of Data Analysis, Moscow, Russia*
[42] *Budker Institute of Nuclear Physics (SB RAS), Novosibirsk, Russia*
[43] *Institute for High Energy Physics NRC Kurchatov Institute (IHEP NRC KI), Protvino, Russia, Protvino, Russia*
[44] *ICCUB, Universitat de Barcelona, Barcelona, Spain*
[45] *Instituto Galego de Física de Altas Enerxías (IGFAE), Universidade de Santiago de Compostela, Santiago de Compostela, Spain*

[46] Instituto de Fisica Corpuscular, Centro Mixto Universidad de Valencia - CSIC, Valencia, Spain
[47] European Organization for Nuclear Research (CERN), Geneva, Switzerland
[48] Institute of Physics, Ecole Polytechnique Fédérale de Lausanne (EPFL), Lausanne, Switzerland
[49] Physik-Institut, Universität Zürich, Zürich, Switzerland
[50] NSC Kharkiv Institute of Physics and Technology (NSC KIPT), Kharkiv, Ukraine
[51] Institute for Nuclear Research of the National Academy of Sciences (KINR), Kyiv, Ukraine
[52] University of Birmingham, Birmingham, United Kingdom
[53] H.H. Wills Physics Laboratory, University of Bristol, Bristol, United Kingdom
[54] Cavendish Laboratory, University of Cambridge, Cambridge, United Kingdom
[55] Department of Physics, University of Warwick, Coventry, United Kingdom
[56] STFC Rutherford Appleton Laboratory, Didcot, United Kingdom
[57] School of Physics and Astronomy, University of Edinburgh, Edinburgh, United Kingdom
[58] School of Physics and Astronomy, University of Glasgow, Glasgow, United Kingdom
[59] Oliver Lodge Laboratory, University of Liverpool, Liverpool, United Kingdom
[60] Imperial College London, London, United Kingdom
[61] Department of Physics and Astronomy, University of Manchester, Manchester, United Kingdom
[62] Department of Physics, University of Oxford, Oxford, United Kingdom
[63] Massachusetts Institute of Technology, Cambridge, MA, United States
[64] University of Cincinnati, Cincinnati, OH, United States
[65] University of Maryland, College Park, MD, United States
[66] Los Alamos National Laboratory (LANL), Los Alamos, United States
[67] Syracuse University, Syracuse, NY, United States
[68] Laboratory of Mathematical and Subatomic Physics , Constantine, Algeria, associated to [2]
[69] School of Physics and Astronomy, Monash University, Melbourne, Australia, associated to [55]
[70] Pontifícia Universidade Católica do Rio de Janeiro (PUC-Rio), Rio de Janeiro, Brazil, associated to [2]
[71] Guangdong Provencial Key Laboratory of Nuclear Science, Institute of Quantum Matter, South China Normal University, Guangzhou, China, associated to [3]
[72] School of Physics and Technology, Wuhan University, Wuhan, China, associated to [3]
[73] Departamento de Fisica , Universidad Nacional de Colombia, Bogota, Colombia, associated to [12]
[74] Institut für Physik, Universität Rostock, Rostock, Germany, associated to [16]
[75] Van Swinderen Institute, University of Groningen, Groningen, Netherlands, associated to [31]
[76] National Research Centre Kurchatov Institute, Moscow, Russia, associated to [38]
[77] National University of Science and Technology "MISIS", Moscow, Russia, associated to [38]
[78] National Research University Higher School of Economics, Moscow, Russia, associated to [41]
[79] National Research Tomsk Polytechnic University, Tomsk, Russia, associated to [38]
[80] University of Michigan, Ann Arbor, United States, associated to [67]

[a] Universidade Federal do Triângulo Mineiro (UFTM), Uberaba-MG, Brazil
[b] Laboratoire Leprince-Ringuet, Palaiseau, France
[c] P.N. Lebedev Physical Institute, Russian Academy of Science (LPI RAS), Moscow, Russia
[d] Università di Bari, Bari, Italy
[e] Università di Bologna, Bologna, Italy
[f] Università di Cagliari, Cagliari, Italy
[g] Università di Ferrara, Ferrara, Italy
[h] Università di Genova, Genova, Italy
[i] Università di Milano Bicocca, Milano, Italy
[j] Università di Roma Tor Vergata, Roma, Italy
[k] Università di Roma La Sapienza, Roma, Italy
[l] AGH - University of Science and Technology, Faculty of Computer Science, Electronics and Telecommunications, Kraków, Poland
[m] DS4DS, La Salle, Universitat Ramon Llull, Barcelona, Spain
[n] Hanoi University of Science, Hanoi, Vietnam
[o] Università di Padova, Padova, Italy
[p] Università di Pisa, Pisa, Italy
[q] Università degli Studi di Milano, Milano, Italy
[r] Università di Urbino, Urbino, Italy
[s] Università della Basilicata, Potenza, Italy

[t] Scuola Normale Superiore, Pisa, Italy
[u] Università di Modena e Reggio Emilia, Modena, Italy
[v] Università di Siena, Siena, Italy
[w] MSU - Iligan Institute of Technology (MSU-IIT), Iligan, Philippines
[x] Novosibirsk State University, Novosibirsk, Russia
[y] INFN Sezione di Trieste, Trieste, Italy
[z] School of Physics and Information Technology, Shaanxi Normal University (SNNU), Xi'an, China
[aa] Physics and Micro Electronic College, Hunan University, Changsha City, China
[ab] Universidad Nacional Autonoma de Honduras, Tegucigalpa, Honduras